10.2514/6.2016-1165

AIAA SciTech Forum
4-8 January 2016, San Diego, California, USA
54th AIAA Aerospace Sciences Meeting

Swept shock/corner flow interactions

Rohan R. Morajkar* and Mirko Gamba†
Department of Aerospace Engineering, University of Michigan, Ann Arbor, MI 48105

The interaction between a swept shock and the secondary flows present in the corners of a supersonic channel flow is experimentally investigated. Such an interaction presents an additional type of unit problem different than the isolated fin-type swept shock/boundary layer interaction. Stereo PIV measurements were conducted perpendicular to the principal flow direction in order to capture the secondary flows characteristic of such an interaction. Various parameters, such as vorticity, probability of flow separation, separation strength and friction coefficient are evaluated. The region of strongest separation in the flowfield generated by a coupled 3D SBLI was found to be at the location of the interaction between the vortex induced by the swept shock and the corner vortex developed in the corner of the channel. In this study, we attempt at explaining the mechanisms responsible for the observed separation.

Nomenclature

x	=	principal flow direction
y	=	direction tangent to the bottom-wall pointing leftwards looking downstream
z	=	direction perpendicular to x and y completing the right handed co-ordinate system
U	=	principal flow velocity or flow velocity in x-direction
V	=	flow velocity in y-direction
W	=	flow velocity in z-direction
u	=	instantaneous velocity in x-direction
v	=	instantaneous velocity in y-direction
w	=	instantaneous velocity in z-direction
t	=	wall tangential direction
n	=	wall normal direction
δ_{99}	=	99 % boundary layer thickness
ω_{RR}	=	rigid rotation vorticity
C_f	=	coefficient of friction

Subscripts:

x,y,z	=	derivative in respective direction
w	=	quantity evaluated at the wall
∞	=	quantity evaluated in freestream

Superscripts:

$\prime$	=	fluctuation quantity
$+$	=	inner wall scale
$*$	=	Corrected using van Driest (1951) compressible scaling

I. Introduction

It is vital to understand the effect of the interaction between the secondary flows that develop in the corner of a ducted supersonic flow and an incident swept shock on the properties of the core flow and separated flow regions. This type of interaction can be found in many shock wave/boundary layer interaction (SBLI) situations, as for example observed in air intake systems for supersonic/hypersonic aircrafts. This study is motivated by the substantial effect corner flows have on global features, such as flow separation, as observed in previous studies. Previous studies describing the importance of corner flows on SBLIs have been reported for various configurations such as those by

*Graduate Student Research Assistant, AIAA Student Member, rohanrm@umich.edu
†Assistant Professor, AIAA Member, mirkog@umich.edu

Batcho and Sullivan [1], Cresci et al. [2]; recently, the oil flow studies conducted by Bruce et al. [3], Burton and Babinsky [4], Eagle et al. [5], and Morajkar et al [6] have elucidated the flow footprint on the walls and given an insight on the resulting global flow structure. Reda and Murphy [7] were amongst the first to note the regions of separations observed near the corners in such flows. However, most of these studies focused on the qualitative aspect of these flows using flow visualizations and/or pressure measurements, while in some of the studies Laser Doppler velocimetry (LDV) [3, 4] have been reported. While pitot pressure measurements are intrusive and may disturb the flow structure, LDV produces results at discrete points. In the current study a set of high-resolution quantitative velocity measurements in the region of the interaction between the swept shock and the corner flow is considered. These measure will enable us to identify the flow structure and to identify the mechanisms responsible for the strong incipient flow separation observed in this region [6, 8].

This study is a part of a broader effort to investigate the 3D shock-boundary layer interactions, which couple the three classical isolated unit physics problems: an incident oblique SBLI, a swept SBLI and corner-shock interaction. These unit physics problems have been considered in isolation in many previous studies [9, 10, 11, 12, 13, 14]. Three-dimensional interactions has been discussed by Helmer et al. [15], Eagle[16], Humble et al.[17] and Morajkar et al. [6, 8]. During our previous studies of 3D SBLIs [6, 8], we found that the vortex induced by the swept shock may interact with the secondary corner flow causing strong incipient flow separations, which in turn, can affect the primary flow. Thus, it is necessary that this interaction between swept shock and the corner region be studied further. We use high-resolution stereo particle image velocimetry (sPIV) to measure the streamwise evolution of the corner flow properties in our Mach 2.75 channel flow that we have extensively used in our 3D SBLI work[5, 18, 16, 6, 8]. We consider a parametric study where the angle of deflection is varied in order to study the effect of shock strength on flow separation and compare it to the case of an isolated (i.e., not affected by 3D effects) incident SBLI [19]. Here we report initial measurements in a 6° angle of attack wedge at Mach of 2.75 [16, 6], which falls in the incipient separation zone of the Korkegi diagram. However, we observed strong intermittent separation on the side-wall [6, 8] which is primarily due to interaction of the swept shock system with the corner flows. In this work we present a hypothesis explaining why the flow separates where it separates on the side-wall.

II. Experimental Setup

A. Wind Tunnel setup

The work presented in this article is a result of the experiments carried out at the Michigan Glass Wind Tunnel (GWT) facility. A schematic diagram of the configuration used in the study is shown in Figure 1a. It is a low aspect ratio suction supersonic wind tunnel $57.2\text{mm} \times 69.3\text{mm}$ ($2.25\text{in} \times 2.75\text{in}$) in cross-section currently configured to operate nominally at Mach 2.75 with stagnation pressure and temperature of 98.1kPa and 294K, respectively. The effective Mach number is approximately 2.72. The tunnel is composed of a one-sided two-dimensional converging-diverging nozzle followed by a constant area test section. This design was selected to produce an equilibrium flat plate boundary layer [20] in an attempt to minimize pressure gradients history effects and Görtler vortices on the boundary layer developing on the bottom-wall (floor) of the wind tunnel. We use the same coordinate system of our previous SBLI work [6, 18, 5]. In particular, the origin of the coordinate system is centered at the location of the leading edge of the full-span 6° shock generator wedge (which is about 481.5mm downstream of the nozzle throat) used in our 3D SBLI work. The details of the 6° shock generator wedge are shown in Figure 1b. The nominal location of oblique shock impinging on the bottom-wall boundary layer at the centerline of the wind tunnel ($y = 28.6\text{mm}$) is about $x = 95\text{mm}$. The unit Reynolds number of the flow is $8.9 \times 10^6/\text{m}$ with an incoming boundary layer thickness (δ_{99}) of 10mm measured at $x = 75.5\text{mm}$ and $y = 28.6\text{mm}$ in an empty tunnel [20]. The pressure gradient parameter defined as $\beta = \frac{\delta}{(\rho U^2)} \frac{\partial P}{\partial x}$ was calculated from side-wall static pressure measurements conducted in the empty tunnel at half the tunnel height. The value of this parameter was found to be 5×10^{-4} for this experiment. A complete summary of the experimental conditions along with their respective uncertainties is provided in A. Optical access to the test section is provided from both sides of the wind tunnel by glass windows that run along the whole length of the wind tunnel, including the nozzle throat region.

B. Stereo Particle Image Velocimetry (SPIV)

SPIV measurements were performed. Two interline transfer CCD cameras (LaVision Flowmaster) recording at 3.33 Hz with a resolution of 1280×1024 pixel were used for the imaging. The cameras were placed in a stereoscopic, forward-scattering configuration oriented at 33° with respect to the measurement plane. The cameras feature a minimum interframe time delay of about 500 ns. The double-pulse illumination of the flow is provided by a pair of low repetition rate, frequency-doubled Nd:YAG lasers producing an output of 532 nm beam with a total energy of 200 mJ/pulse.

Mach number M^1_∞	2.71 ± 0.1	Static Temperature T^3_∞	$119 \pm 1\text{K}$
Mach number M^2_∞	2.72 ± 0.03	Test section height[4]	$69.3 \pm 0.2\text{mm}$
Free Stream velocity U^3_∞	$593 \pm 21\text{m/s}$	Test section width[4]	$57.2 \pm 0.1\text{mm}$
Stagnation Pressure P^4_0	$98.1 \pm 1\text{kPa}$	Throat height[4]	$18.4 \pm 0.1\text{mm}$
Stagnation Temperature T^4_0	$294 \pm 2\text{K}$	Throat to origin distance[4]	$481.5 \pm 1\text{mm}$
Wall Static Pressure $P\ (x = -85\text{mm})^4$	$4.15 \pm 0.6\text{kPa}$		

[1] Computed from a direct measure of stagnation and static pressure assuming isentropic expansion ($\gamma = 1.4$).
[2] Computed from a direct measure of the ratio of stagnation pressure and test section pitot pressure ($\gamma = 1.4$).
[3] Uncertainty estimated from error propagation rule.
[4] Uncertainty includes both measurement accuracy and day-to-day variability.

Table 1. Summary of wind tunnel conditions.

The lasers are triggered at 10 Hz with a time delay of 650 ns in between the two pulses and pulse duration of 10 ns. The delay is measured with a ThorLabs DT10A/M photodiode that has a 1 ns response time and a LeCroy Waverunner 6030 350 MHz digital oscilloscope, and then ensured by adjusting the time delay between the trigger signals to the laser pair. In order to minimize particle dropout and volumetric effects, laser sheet thickness is set using expanding-collimating optics to approximately 4 times the out-of-plane displacement of a particle within the measurement domain as suggested by Adrian and Westerweel [21]. The beam width was measured to be $1.45 \pm 0.25\text{mm}$, which is approximately 3.6 times the particle displacement (approx. $400\mu\text{m}$) in 650 ns at the free-stream speed.

Particle seeding of the flow was generated by a TDA-4B portable Laskin nozzle aerosol. The generator consists of an array of six Laskin nozzles that create poly-dispersed sub-micron particles using Poly-Alpha Olefin (PAO) oil with density of 819kg/m^3. The LaVision DaVis 8 software is used for the acquisition of the measurement and processing of the data. The three-component velocity fields are reduced from the particle images using Davis 8. A multi-pass with reducing interrogation window size is used. Two passes were conducted using an interrogation window size of 64x64 pixels with a 50% overlap. The final size of the interrogation windows after two further passes was 32x32 pixels with an overlap of 75%, which corresponds to a projected physical size of about 0.47 mm x 0.47 mm and a vector resolution of about 0.15 mm x 0.15mm spanning a physical region of 17 mm x 17 mm. Post processing within multiple passes included deleting a vector if its correlation value was less than 0.8 as well as removing groups with less than 4 vectors. Post processing was also conducted once all the passes were completed by removing vectors with a peak ratio (Q) less than 1.2. Laser sheets were oriented perpendicular to the flow, spanning a fraction the cross-section of the tunnel. Multiple such images (about 1000 instances at each measurement location) were recorded to construct distributions of various flow properties.

The data (each snapshot/instantaneous) was further validated in Matlab as per the criteria proposed by Nogueira et al. [22]. The missing data was then interpolated using a fourth order differential equation for interpolating data [23]. The method leaves all known values intact. The data was filtered using a 5×5 Gaussian filter which corresponds to a a physical span of about $(0.75\text{mm} \times 0.75\text{mm})$ with a standard deviation corresponding to 2.5 vector spacing. All of the SPIV data was analyzed using PIVMAT [24] modified to use least squared difference scheme for computing derivatives except at the edges where forward and/or backward differencing was used.

Measurements are made on multiple planes in three orthogonal orientations (streamwise/vertical, SV; streamwise/horizontal, SH; and transverse/vertical, TV, planes) which have been described in our previous works [25, 26]. A schematic showing the location and orientation of planes where data was recorded is shown in Figure 2. Measurements in TV configuration were also made in the tunnel without the wedge to study the secondary flows in the corner which exist without any presence of shock at $x = -100\text{mm}$, $x = -50\text{mm}$ and $x = 75\text{mm}$. These flowfields are discussed in detail in our other work [27].

III. Description of mean fields

A schematic diagram of the flow structure associated with the problem investigated here in the region of interest is shown in Figure 3. We are interested in the region where the vortex induced by the incoming swept shock on the side-wall interacts with the corner flow. As per the work of Alvi and Settles [11], a swept SBLI should produce no separation for a normal Mach number of 1.17 and a static pressure jump of 2.2; yet flow separation is observed where the fluid is convected away from the side-wall as a result of the secondary flow structures present in the corner. The effect of three dimensionality can also be observed by comparing the streamwise core flow area of the current

configuration with inviscid theory as shown in Figure 4. The core flow area is defined as the area enclosed by the iso-contour of $0.1U_\infty$ on the contour map of mean magnitude of in-plane flow vectors.

The complete features of this case (6° deflection) are discussed in our previous works [16, 8]. Planes TV5 and TV9 (that lie at $x = 75\text{mm}$ and $x = 96\text{mm}$, respectively) will be discussed in detail and they are take as plans containing the representative flow structures. The choice of these planes allows us to analyze the secondary flow patterns in the upstream influence region of the SBLI and at the nominal interaction location of the incident SBLI. Also, data in the corner region of the undisturbed duct flow is available at a location of $x = 75\text{mm}$ for comparison [27]. Separation bubble height profile as defined by Piponniau et al. [28] and Souverein et al. [29] is used to compute the profile of the region affected by flow separation for each instantaneous velocity field in the dataset. The instantaneous separation bubble profiles are then averaged to obtain the mean separation bubble profile. The mean separation bubble cross-section profile as seen in the TV9 plane is shown in Figure 5a. The figure represents the flowfield such that the y-axis forms the bottom-wall and the z-axis forms the side-wall, with the net flow being out of the plane of the page. As we can see there is a bulge of low momentum flow extending towards the core flow from the side-wall developed at $z = 7\text{mm}$, while the high momentum fluid is seen to convect towards the corner near bottom-wall at $y = 13\text{mm}$. The separation bubble is seen to be within the momentum deficit region with its highest point being at about $z = 7\text{mm}$. The sonic line is seen to follow the iso-tach lines associated with this pattern. Separation area was computed at multiple TV planes and the streamwise variation of separation area is shown in Figure 6. It can be seen that the side-wall separation is stronger than the bottom-wall separation (larger area).

A map of the probability of observing reversed flow ($u \leq 0$) was constructed from the different data planes collected and is shown in Figure 7. It can be observed that the strongest separation is always observed at about $7 < z < 10\text{mm}$ along the side-wall. This is the region where the secondary flow associated with the corner exists and possibly, the strong separation observed here is an effect of the corner interacting with the secondary flow associated with the incoming swept shock.

Because the flow in the corner is dominated by heavy shear and strain, traditional Cauchy Stokes' decomposition of motion into symmetric part (shear) and anti-symmetric (vorticity) is insufficient. The shear and strain mask the vorticity associated with the rigid rotation of vortex tubes and makes identifying the corner vortices difficult. Thus, a planar surrogate of the Triple Decomposition of Motion (TDM) [30] was used to determine only the part of vorticity associated with rigid-body rotation (ω_{RR}), which makes identifying the corner vortices more clear. The TDM field obtained from the mean vector field of TV9 is shown in Figure 5b. We can observe that the vortex field is primarily characterized by two vortex systems: opposing vortices A and B forming the corner flow vortex system [31, 32, 33, 34] and vortex C being induced by the incoming swept shock [11, 13]. Comparing Figures 5a and 5b we can observe that the separation is strongest at the location where the in-plane vectors are being directed away from the side-wall as a combined action of vortex B and C. A global flow structure was constructed from the rigid rotation vorticity fields obtained from other data planes which is shown in Figure 8 [8].

IV. Hypothesis

Shabaka et al. [35] studied in detail the effects of having a vortex close to a bounding surface in a flow. A vortex that exists close to a bounding surface transports lower momentum fluid from the wall to the core on the downwash side, thus modifying the velocity profile to be less full, while transports higher momentum fluid from the core towards the wall on the upwash other side, thus making the velocity profile fuller. This result in an increase in skin friction coefficient (C_f) on the fuller side, and a decrease on the other side. The side with net lower C_f is more susceptible to flow separation than the rest of the flow, while the region of maximum C_f represents a region with higher resistance to flow separation.

In the case two (counter-rotating) vortices lie in close proximity to each other, two regions arise: the region of common flow upwash [36] and the region of common flow downwash. The case where flow upwash exists is associated with an intensification of the decrease in C_f because the two vortices increase the strength of the low momentum flow transport away from the wall. The SBLI problem studied here exists at the location where the swept shock interacts with the corner vortex along the side-wall. This results in strong flow separation (see Figures 5a, 6, and 7). This is associated with a point of minimum C_f, which makes the flow more prone to separation. In the opposite case where downwash exists, the flow has a higher resistance to separation and corresponds to a maximum in C_f. The case of downwash is observed in the corner of a rectangular duct which features counter-rotating corner vortices with common flow towards the corner.

A. Lines of potential separation and reattachment

A line of potential separation (SL) is defined as the locus of local minima of C_f or maxima of deficit of mean streamwise momentum (caused by vortical low momentum transport away from the wall) along the wall, and it identifies a line along which the flow would begin to separate or is characterized by intermittent separation or in general, has the highest tendency to separate. Such a line would be typical of a configuration of a streamwise-oriented vortex tube near a wall as shown in Figure 9.

As seen in Figure 9, a vortex tube that exists close to a wall and hence to a boundary layer, would draw the lower momentum fluid from near the wall towards the freestream on one side, thus increasing the potential of flow to separate. The locus along which this effect is the strongest is referred to as the line of potential separation (SL). If a counter-rotating vortex exists, this tendency would be reinforced in the region of common upwash. Here, the line of potential separation of relatively weak isolated vortices is referred to as SL and denoted by a dotted line, while that caused by adverse pressure gradient or close proximity of two counter rotating vortices is referred to as SL and denoted by a solid line. Conversely, on the other side of the vortex tube, higher momentum fluid from the free stream is drawn towards the wall, thus decreasing the tendency to separate. The region is here referred to as the line of reattachment (RL). The RL also corresponds to the line of local maxima of C_f or maxima in streamwise momentum profile near the wall (caused by vortical high momentum transport towards the wall). A schematic diagram showing the map of lines of potential separation and reattachment of the SBLI problem considered here are shown in Figure 10 and are extracted by inspection of the system of vortices detected in the study of this SBLI case [8].

In Figure 10 SL1 is a result of the adverse pressure gradient of the swept shock and the associated vortex C. The vortex C transports higher momentum fluid towards the side-wall causing a reattachment line RL1. SL'1 (dashed line becoming solid once it encounters adverse pressure gradient due to the shock) is caused by the corner vortex B, which then merges into SL1 producing a stronger potential to separate as a result of the close proximity of near wall counter-rotating vortices B and C as well as the adverse pressure gradient due to the shock as was seen in Figure 8.

Both the corner vortices A and B convect high-momentum fluid towards the corner of the tunnel producing RL2. SL'2 (dashed line) is caused only by the relatively weak corner vortex A. SL'2 merges into a stronger SL2, which is a result of the interaction between two counter-rotating vortices A and D and an adverse pressure gradient caused by the shock. Vortex D and its counterpart which would exist in the other half of the domain, would form a counter-rotating pair which would form a strong reattachment line (RL4) on the centerline of the tunnel if the spacing were sufficiently small. SL3 is produced by the incident oblique shock and the span-wise vortex which exists at the foot of this shock, while RL3 is the reattachment line caused by this vortex. Based on this view, the potential to separate in the SBLI region would be greatest where most of the potential separation lines are in close proximity to each other as shown in Figure 10. In the case shown here, it is the region where the swept shock vortex C is closest to the bottom-wall, and thus closest to the spanwise vortex and the corner vortices A and B. Such region would be found around $x = 100\text{mm}$. Thus, the sudden increase in separation bubble cross-section area in Figure 6 may be attributed to this phenomenon of vortex interaction.

Thus, it would be helpful to define the separation potential parameter (ζ) which would quantify the likeliness of the flow to separate at a given location on the wall. It is highly likely that ζ is a function of the local C_f, which takes into consideration the viscous effects; the local non-dimensional pressure gradient (β); the boundary layer shape factor H, which describes the fullness of the boundary layer and hence the concentration of high momentum fluid in the proximity of the surface; and a characteristic Mach number, which would account for the compressibility of the flow.

In this work we will explore this hypothesis from the set of measurements already available, and we will extend it to the new set of measurements on additional incident SBLI configurations we are currently conducting.

V. Efforts to support hypothesis

Because the likelihood of flow separation is believe to be associated with the large scale vertical structures present in the flowfield, we extract additional flow properties after lowpass filtering the measured vector fields to generate an equivalent representation that captures solely the largest scale features of the flow. In practice, the lowpass filtering operation was carried out with a moving average filter of size of 0.5 mm $\times$ 0.5 mm operation. This approach follows our companion study [27] of the structure of the corner flow by first performing a scale decomposition, where an instantaneous field is decomposed into a large and a small scale contributions. It is the large scale contribution that is responsible for the evolution of the corner vortex system; while the small scale captures the underlying turbulent features. The large scale vortex features were then extracted after applying the the TDM, from which rigid rotation vorticity ω_{RR} is extracted. The identification of the corner vortex then followed using the definition introduced in the companion work [27].

The mean flowfield obtained at $x = 75\text{mm}$ in the empty tunnel is shown in Figure 11a. The wall normal mean streamwise velocity profiles are shown in Figures 11b & 11c. The deficit in the streamwise velocity profile near side-wall ($y = 5\text{mm}$) created due to the negative corner vortex can be observed in Figure 11b at about ($z = 5 - 10\text{mm}$). As per our hypothesis this region would be a candidate for the existence of a line of separation potential.

The effect of momentum transport due to corner vortices is observed in the streamwise velocity gradients. The velocity gradient fields overlapped with iso-contours of mean rigid rotation vorticity are shown in Figures 12a and 12b. The negative corner vortex shown by the white iso-contour lines convects lower momentum fluid away from the side-wall creating a decrease in the $U-$velocity as we traverse in $+z$-direction from the bottom-wall near the side-wall. This effect is observed as a dip in the $U(z)$ profiles shown in Figure 11b near side-wall ($y = 2.5$ &7.5mm) and thus, produces a negative $\partial U/\partial z$ at the location of the vortex in Figure 12b. A similar effect is observed with the positive corner vortex near the bottom-wall. Since the $\partial U/\partial y$ field is positive at the location where $\partial U/\partial z$ is negative and vice versa, the product of $\partial U/\partial y$ and $\partial U/\partial z$ would identify the region with momentum deficit in Figure 12c. Thus, observing Figure 12c with reference to a vertical line (i.e., any line in the range $y = 0 - 5\text{mm}$) near the side-wall, the U velocity profile continues to increase until we encounter the region with negative (blue) $(\partial U/\partial y)(\partial U/\partial z)$, it then begins to decrease until the end of the region of negative $(\partial U/\partial y)(\partial U/\partial z)$. The deficit in the streamwise momentum is the highest between the end of the region of negative $(\partial U/\partial y)(\partial U/\partial z)$ and the start of the region of positive $(\partial U/\partial y)(\partial U/\partial z)$. This location (around $z = 8\text{mm}$) would mark a point on the line of separation potential and would be most likely to separate should an adverse pressure gradient be applied (e.g., a shock wave sweeping through this region). By comparison with the incident SBLI data at this location, it is found that this is indeed the case. We overlay the mean side-wall separation bubble profile (yellow line) found from the 6° incident SBLI case at this measurement plane to the data from the empty tunnel of Figure 12c. In the incident SBLI case, an adverse pressure gradient is created by the incident shock and its influence is felt upstream through the subsonic region of the boundary layer[37]. It can thus be concluded that the upstream side-wall separation observed in the incident SBLI study may be primarily a consequence of the structure of the corner flow region where the flow at the corner is more likely to separate as the adverse pressure due to the incident shock is (externally) applied to the corner flowfield.

The region with streamwise velocity component less than 25m/s ($u \leqslant 25\text{m/s}$) was considered to be separated flow while the maximum extent the separated flow region away from the wall was defined as the height of separation bubble (H) [25]. The separation bubble height was then used to correlate the likelihood of flow separation with the presence of the corner vortex system disturbed by the pressure gradient imposed by the incident shock. The z-location of the negative corner vortex center in the empty tunnel was compared with the z-location of the point of maximum separation height (H) on the side-wall separation region on the $x = 75\text{mm}$ measurement plane. Histograms of these two quantities are shown in Figure 13. It can be seen from the figure that the most probable location of the negative vortex in the empty tunnel is approximately the same to the most probable position of the point of maximum separation height. We take this as an initial indication supporting the hypothesis that the location of separation depends on the vortex arrangement of the flow in the corner region. However, additional work is necessary to fully test this hypothesis. In this regard, additional analysis is being conducted to further evaluate this hypothesis by constructing conditional statistics on the point of separation relative to the instantaneous flow structure in the corner (particularly on the position and strength of the corner vortex pair).

VI. Conclusions

The $M = 2.75$, 6° angle of deflection incident SBLI case was studied using sPIV measurements to quantify the importance of the interaction of the swept shock with the corner flows. An hypothesis explaining the underlying mechanism of flow separation due to vortical momentum transport was put forth and initially tested; but additional analysis is required to fully test this hypothesis. The flow structure obtained from empty tunnel measurements was used to predict the location of most probably observing flow separation in the case an adverse pressure gradient would be applied, as for example when the swept-shock on the side wall reaches the corner region. The predicted point of separation on the side-wall agrees with the observed point of separation from the incident SBLI measurements, thus providing some initial support to the proposed mechanism. This work is part of a study currently underway aimed to investigate the role corner-induced secondary flows on flow separation observed in 3D incident SBLIs.

Acknowledgments

The authors would like to thank Robin L. Klomparens, Prof. James F. Driscoll, and Dr. Jack Benek, Wright Patterson Air Force Base for their valuable inputs. We also acknowledge Dr. Derek Dale for putting forth this LaTeX template.

References

[1] Batcho, P. and Sullivan, J., "The 3-D Flowfield in a Supersonic Shock Boundary Layer Corner Interaction," *AIAA 26th Aerospace Sciences Meeting*, Reno, Nevada, 1988.

[2] Cresci, R. J., Rubin, S. G., Nardo, C. T., and Lin, T. C., "Hypersonic Interaction along a Rectangular Corner," *AIAA Journal*, Vol. 7, No. 12, 1969, pp. 2241–2247.

[3] Bruce, P. J. K., Burton, D. M. F., Titchener, N. a., and Babinsky, H., "Corner effect and separation in transonic channel flows," *Journal of Fluid Mechanics*, Vol. 679, may 2011, pp. 247–262.

[4] Burton, D. M. F. and Babinsky, H., "Corner separation effects for normal shock wave/turbulent boundary layer interactions in rectangular channels," *Journal of Fluid Mechanics*, Vol. 707, aug 2012, pp. 287–306.

[5] Eagle, W. E., Driscoll, J. F., and Benek, J. A., "Experimental Investigation of Corner Flows in Rectangular Supersonic Inlets with 3D Shock-Boundary Layer Effects," *49th AIAA Aerospace Sciences Meeting including the New Horizons Forum and Aerospace Exposition*, No. January, American Institute of Aeronautics and Astronautics, Orlando, Florida, 2011, pp. 1–11.

[6] Morajkar, R., Klomparens, R., Eagle, E., Driscoll, J., and Gamba, M., "Flow Separation Associated with 3 - D Shock - Boundary Layer Interaction (SBLI)," *SciTech 2014*, American Institute of Aeronautics and Astronautics, Harbor Town, 2014, pp. 1–13.

[7] Reda, D. C. and Murphy, J. D., "Sidewall Boundary-Layer Influence on Shock Wave / Turbulent Boundary-Layer Interactions," *AIAA Journal*, Vol. 11, No. 10, 1973, pp. 1367–1368.

[8] Morajkar, R. R., Klomparens, R. L., Eagle, W. E., Driscoll, J. F., Gamba, M., and Benek, J. A., "Relationship Between Intermittent Separation and Vortex Structure in a Low - Aspect Ratio 3D Shock Wave - Boundary Layer Interaction," *Submitted to AIAA Journal*.

[9] Délery, J. and Dussauge, J.-P., "Some physical aspects of shock wave/boundary layer interactions," *Shock Waves*, Vol. 19, No. 6, jul 2009, pp. 453–468.

[10] Adamson, T. C. and Messiter, A. F., "ANALYSIS OF TWO- DIMENSIONAL INTERACTIONS BETWEEN SHOCK WAVES AND BOUNDARY LAYERS," *Annu. Rev. Fluid Mech.*, Vol. 12, No. 1939, 1980, pp. 103–138.

[11] Alvi, F. S. and Settles, G. S., "Physical Model of the Swept Shock Wave / Boundary-Layer Interaction Flowfield," *AIAA Journal*, Vol. 30, No. 9, 1992, pp. 2252–2258.

[12] Kubota, H. and Stollery, J. L., "An experimental study of the interaction between a glancing shock wave and a turbulent boundary layer," *Journal of Fluid Mechanics*, Vol. 116, 1982, pp. 431–458.

[13] Panaras, A. G., "The effect of the structure of swept-shock-wave/turbulent-boundary-layer interactions on turbulence modelling," *Journal of Fluid Mechanics*, Vol. 338, may 1997, pp. 203–230.

[14] Knight, D. D., Horstman, C., Bogdonoff, S., and Shapey, B., "Structure of supersonic turbulent flow past a sharp fin," *AIAA Journal*, Vol. 25, No. 10, oct 1987, pp. 1331–1337.

[15] Helmer, D. B., Campo, L. M., and Eaton, J. K., "Three-dimensional features of a Mach 2.1 shock/boundary layer interaction," *Experiments in Fluids*, Vol. 53, No. 5, aug 2012, pp. 1347–1368.

[16] Eagle, W. E. and Driscoll, J. F., "Shock Wave-Boundary Layer Interactions in Rectangular Inlets : 3-D Separation Topology and Critical Points," *Accepted for publication in Journal of Fluid Mechanics*, 2014.

[17] Humble, R. a., Elsinga, G. E., Scarano, F., and van OUDHEUSDEN, B. W., "Three-dimensional instantaneous structure of a shock wave/turbulent boundary layer interaction," *Journal of Fluid Mechanics*, Vol. 622, feb 2009, pp. 33–62.

[18] Eagle, W. E., Driscoll, J. F., and Benek, J. A., "3-D Inlet Shock-Boundary Layer Interactions - PIV Database for the Second SBLI Workshop," *30th AIAA Applied Aerodynamics Conference*, No. June, American Institute of Aeronautics and Astronautics, New Orleans, LA, 2012.

[19] Korkegi, R. H., "A Simple Correlation for Incipient Turbulent Boundary-Layer Separation due to a Skewed Shock Wave," *AIAA Journal*, Vol. 11, No. 11, 1973, pp. 1578–1579.

[20] Lapsa, A. P. and Dahm, W. J. A., "Stereo particle image velocimetry of nonequilibrium turbulence relaxation in a supersonic boundary layer," *Experiments in Fluids*, Vol. 50, No. 1, jun 2010, pp. 89–108.

[21] Adrian, R. J., Christensen, K. T., and Liu, Z., "Analysis and interpretation of instantaneous turbulent velocity fields," *Experiments in Fluids*, Vol. 29, No. 95, 2000, pp. 275–290.

[22] Nogueira, J., Lecuona, A., and Rodriguez, P. A., "Data validation , false vectors correction and derived magnitudes calculation on PIV data," *Measurement Science and Technology*, Vol. 8, 1997, pp. 1493–1501.

[23] D'Errico, J., "inpaint_nans (Interpolation function)," *Matlab Central File Exchange*, Vol. https://www.mathworks.com/matlabcentral/fileexchange/4551-inpaint-nans.

[24] Moisy, F., "PIVMAT toolbox," Vol. http://www.fast.u-psud.fr/pivmat/.

[25] Morajkar, R. R., Klomparens, R. L., Eagle, W. E., Driscoll, J. F., Gamba, M., and Benek, J. A., "Relationship Between Intermittent Separation and Vortex Structure in a Low - Aspect Ratio 3D Shock Wave - Boundary Layer Interaction," *Accepted for publication in AIAA Journal*, pp. 1–52.

[26] Eagle, W. E. and Driscoll, J. F., "Shock waveboundary layer interactions in rectangular inlets: three-dimensional separation topology and critical points," *Journal of Fluid Mechanics*, Vol. 756, sep 2014, pp. 328–353.

[27] Morajkar, R. and Gamba, M., "Turbulence characteristics of supersonic corner flows in a low aspect ratio rectangular channel," *AIAA SciTech 2016*, AIAA, San Diego, Ca, 2016.

[28] Piponniau, S., Dussauge, J. P., Debiève, J. F., and Dupont, P., "A simple model for low-frequency unsteadiness in shock-induced separation," *Journal of Fluid Mechanics*, Vol. 629, jun 2009, pp. 87–108.

[29] Souverein, L. J., Dupont, P., Debiève, J.-F., Van Oudheusden, B. W., and Scarano, F., "Effect of Interaction Strength on Unsteadiness in Shock-Wave-Induced Separations," *AIAA Journal*, Vol. 48, No. 7, jul 2010, pp. 1480–1493.

[30] Kolá, V., "Vortex identification: New requirements and limitations," *International Journal of Heat and Fluid Flow*, Vol. 28, No. 4, aug 2007, pp. 638–652.

[31] Davis, D. O. and Gessner, F. B., "Further Experiments on Supersonic Turbulent Flow Development in a Square Duct," *AIAA JOURNAL*, Vol. 27, No. 8, 1989, pp. 1023–1030.

[32] Gessner, F. B., "The origin of secondary flow in turbulent flow along a corner," *Journal of Fluid Mechanics*, Vol. 58, No. 1, 1972, pp. 1–25.

[33] Gessner, F. B., Eppich, H. M., and Lund, E. G., "Reynolds Number effects on near wall structure of turbulent flow along a streamwise corner," *Near-Wall Turbulent Flows*, 1993, pp. 965–975.

[34] Brundrett, E. and Baines, W. D., "The production and diffusion of vorticity in duct flow," *Journal of Fluid Mechanics*, Vol. 19, No. 3, 1963, pp. 375– 394.

[35] Shabaka, I. M. M. A., Mehta, R. D., and Bradshaw, P., "Longitudinal vortices imbedded in turbulent boundary layers . Part 1 . Single vortex," *Journal of Fluid Mechanics*, Vol. 155, 1985, pp. 37–57.

[36] Mehta, R. D. and Bradshaw, P., "Longitudinal vortices imbedded in turbulent boundary layers Part 2. Vortex pair with 'common flow' upwards," *Journal of Fluid Mechanics*, Vol. 188, 1988, pp. 529–546.

[37] Babinsky, H. and Harvey, John, K., *Shock Wave-Boundary-Layer Interactions*, Cambridge University Press, 2011.

Figures

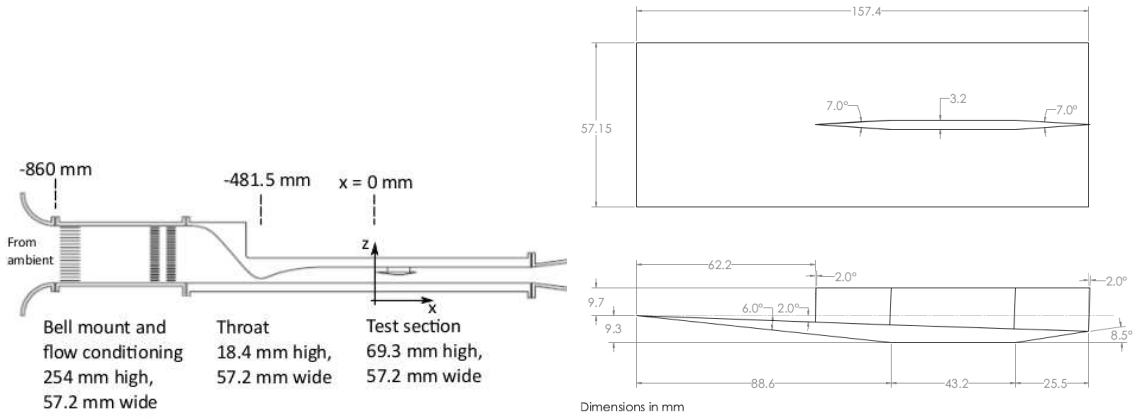

Figure 1. Schematic diagram of the experimental setup: (a) schematic of the wind tunnel; (b) diagram showing the dimensions of the 6° compression surface used to generate the incident shock wave.

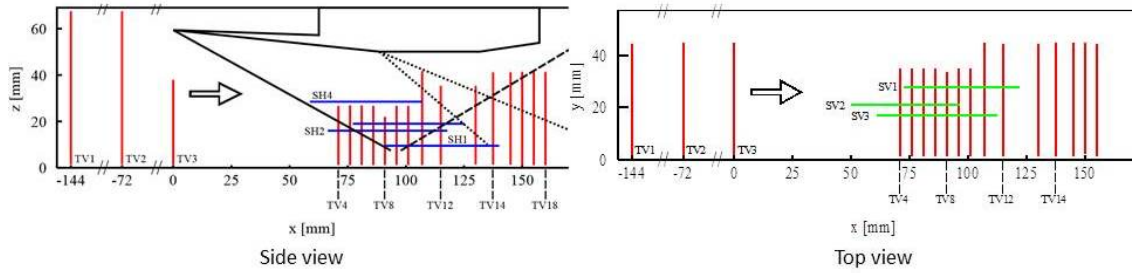

Figure 2. PIV plane locations with respect to the shock generator and calculated shock-expansion fan locations.

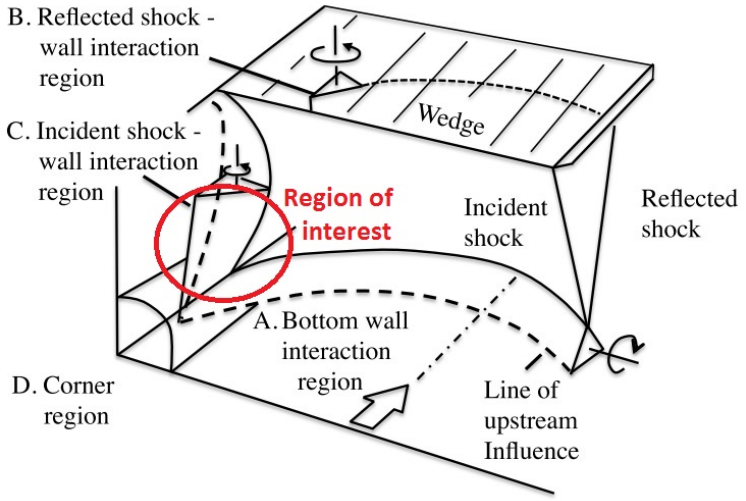

Figure 3. General flow structure schematic with region of interest (from Eagle and Driscoll [16]).

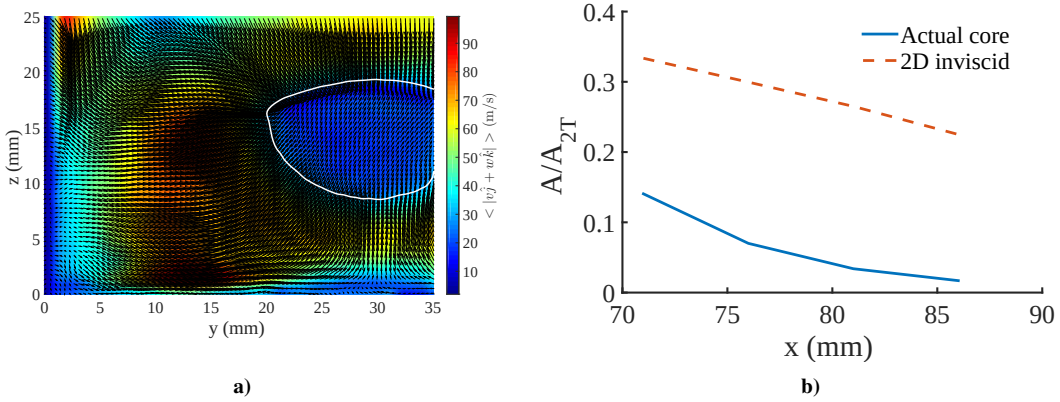

Figure 4. (a) Plot showing mean $|v\hat{j} + w\hat{k}|$ in TV6 with iso contours of $0.1U_\infty$ showing the core flow area; (b) Streamwise evolution of core flow area.

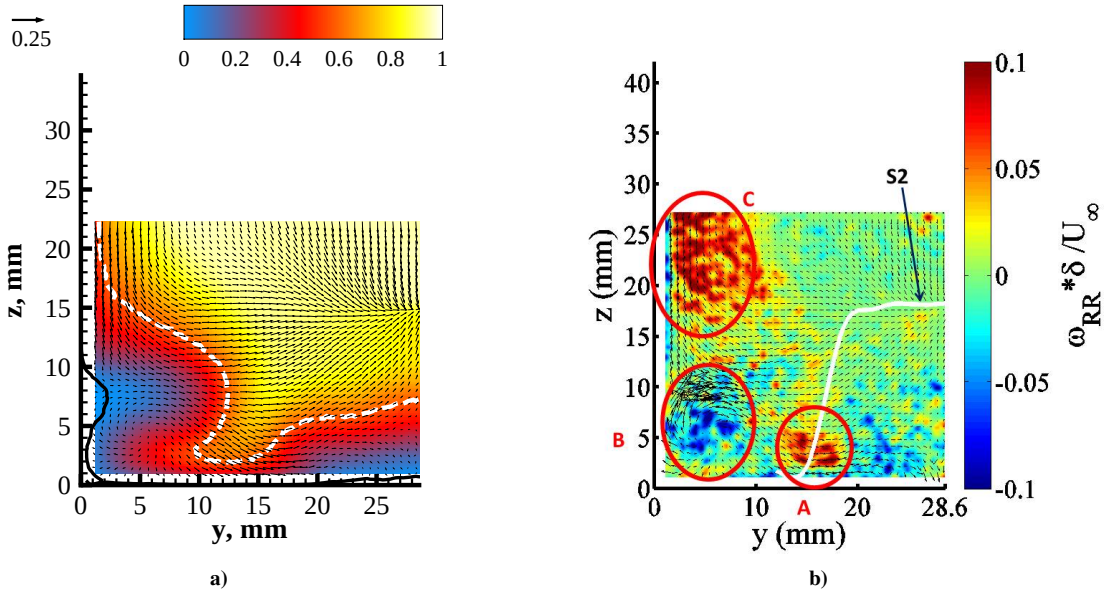

Figure 5. Flow structure observed in TV9: (a) Mean separation bubble profile (black solid line) in TV9 superimposed on the streamwise velocity component contours, in-plane velocity vectors and sonic line (white dashed); (b) Contours of rigid rotation vorticity field in TV9 superimposed by in plane unit vectors and shock trace (solid white line).

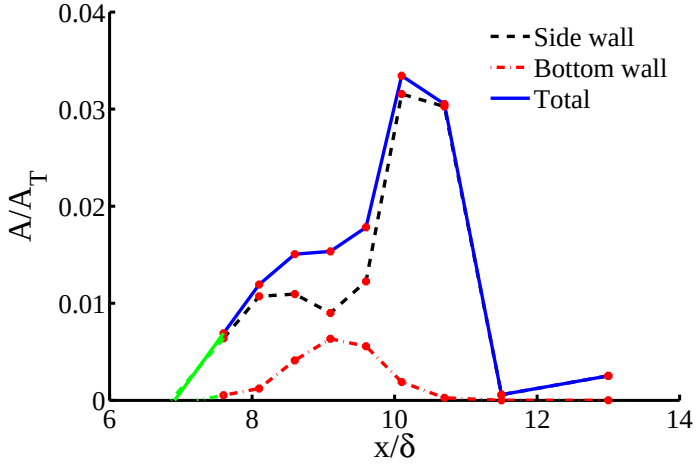

Figure 6. Streamwise distribution of mean separation area (green lines are linear extrapolation of the data.

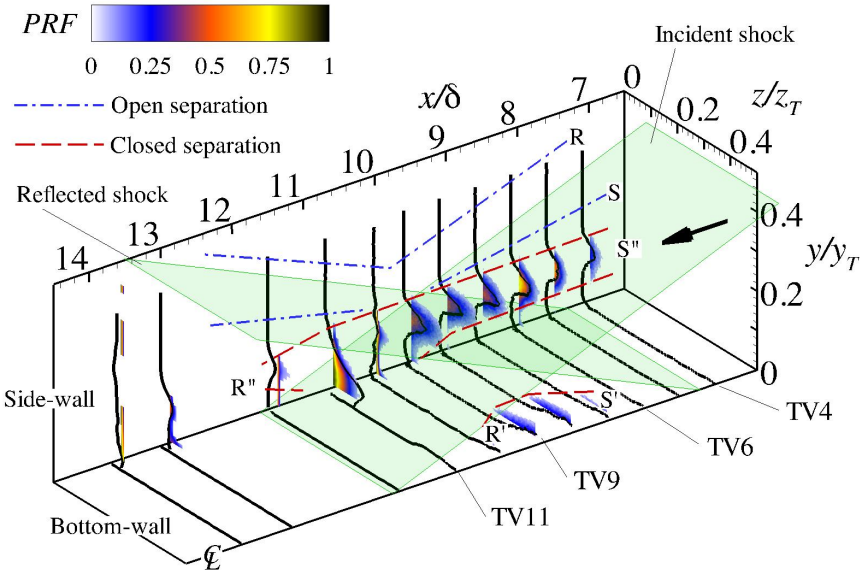

Figure 7. Three-dimensional plot of probability reverse flow (PSF) (color contour) and separation bubble height h (solid line) around the interaction region. S' and R' indicate separation and re-attachment points of the closed separation region on the bottom-wall resulting from the incident shock interaction; S" and R" indicate separation and re-attachment of the closed recirculation region on the side-wall resulting from the corner; S and R are the (approximate) separation lines of the open separation from the swept shock interaction. Incident and reflected shock waves are indicative.

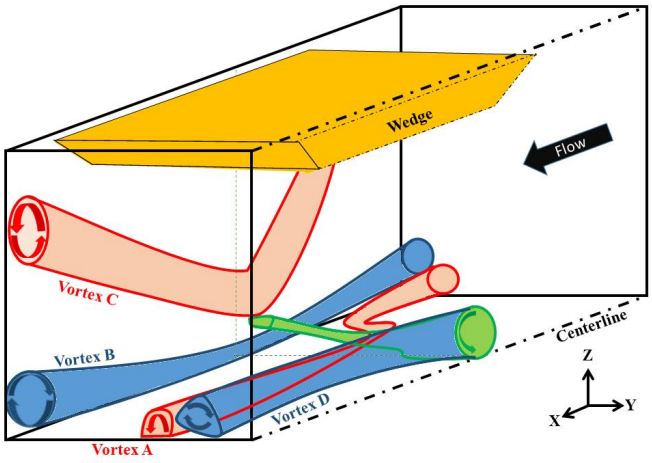

Figure 8. Schematic diagram of the vortex structure associated with the incident 3D SBLI.

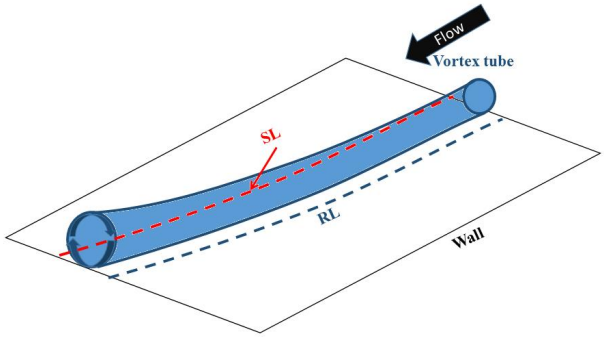

Figure 9. A simple example of potential flow separation and re-attachment lines.

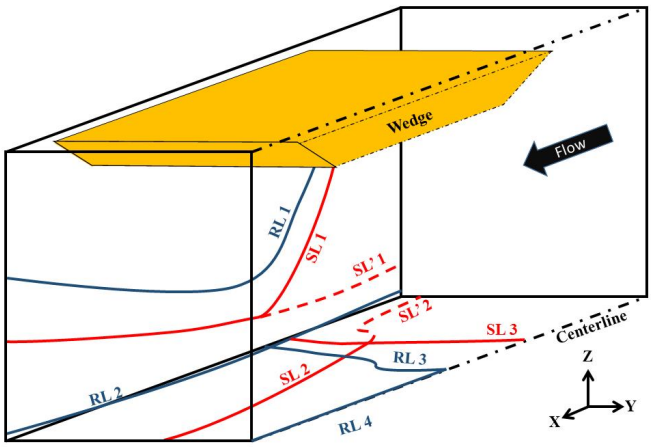

Figure 10. Lines of potential separation and reattachment in an incident 3D SBLI configuration.

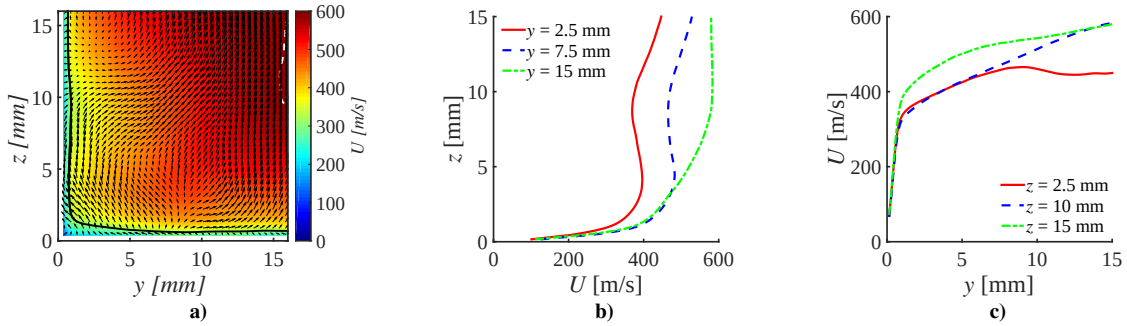

Figure 11. Mean velocity profiles from the data acquired in empty tunnel at $x = 75\text{mm}$. (a) Mean velocity field with in plane velocity components are represented by vectors while the out-of-plane component is shown by the contour map. The solid black line represents the contour for the sonic velocity; (b) $U(z)$; and (c) $U(y)$.

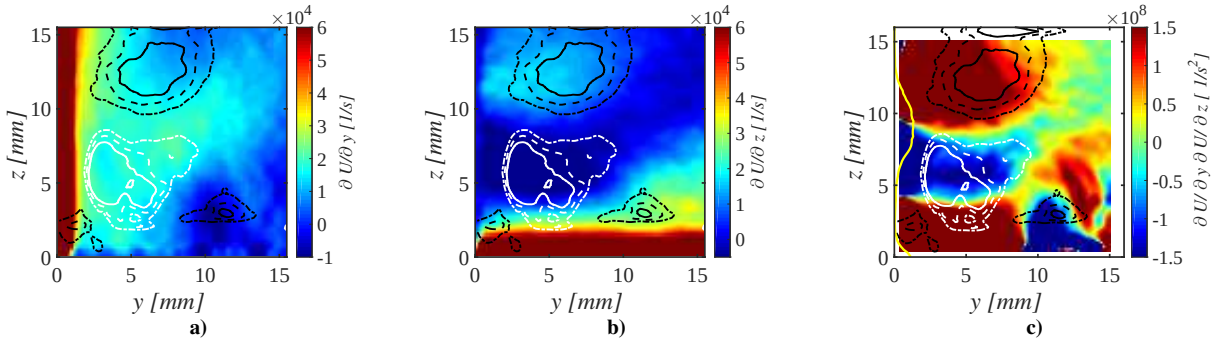

Figure 12. Mean streamwise in-plane velocity gradients and the product of the velocity gradients superimposed with contour lines of mean rigid rotation vorticity at large scales. White iso-contour line: negative vorticity; black iso-contour line: positive vorticity from the empty tunnel data at $x = 75\text{mm}$. (a) $\partial U/\partial y$; (b) $\partial U/\partial z$; and (c) $(\partial U/\partial y)(\partial U/\partial z)$. The yellow line is the mean separation profile obtained from the SBLI data at the same streamwise location.

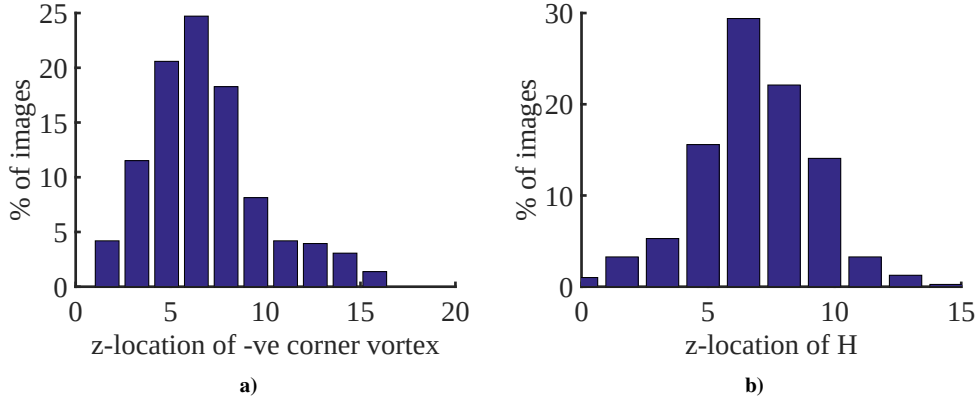

Figure 13. Relation between the location of flow separation bubble and the negative corner vortex in an empty tunnel flowfield: (a) Histogram of z-location of negative corner vortex in empty tunnel at $x = 75\text{mm}$; and (b) Histogram of z-location of the maximum extent of the separation bubble (H) at $x = 76\text{mm}$.